INTERNATIONAL JOURNAL FOR NUMERICAL METHODS IN FLUIDS, VOL. 5, 957–980 (1985)

ON THE NUMERICAL COMPUTATION OF LAMINAR BOUNDARY LAYERS AT A PHASE-CHANGING, GAS–LIQUID INTERFACE

STEPHEN P. KLOTZ* AND ROBERT L. STREET†

Department of Civil Engineering, Stanford University, Stanford, CA 94305, U.S.A.

SUMMARY

The two-dimensional, laminar boundary-layer equations of heat, mass and momentum at a smooth, phase-changing, gas–liquid interface are solved numerically by the Keller Box method. The gas and liquid regimes are embedded in a single marching scheme which computes interfacial parameters implicitly. Results of both self-similar and non-similar boundary-layer computations are presented and effects of mild pressure gradient, a mean current in the liquid, and free-stream vapour concentration on the interfacial parameters are analysed.

In order to assess the accuracy of the method, several self-similar problems are solved by Runge–Kutta integration and results are compared to those obtained by the finite-difference scheme. Agreement is excellent in all cases.

KEY WORDS Gas–liquid Flows Laminar Boundary Layers Heat and Mass Transfer Numerical Methods

1. INTRODUCTION

Many industrial and physical processes require a phase-changing gas–liquid interface for the transport of heat and species from one fluid regime to the other. Among applications related to evaporation, condensation, ablation, pyrolysis and combustion are many problems in which the underlying motion of the liquid is significant and governed by boundary-layer equations similar in form to those which characterize transport in the gas. Despite their obvious importance, however, coupled boundary-layer flows comprise a class of problems for which there is a dearth of experimental data and theoretical analysis because previous investigators have generally focused on either the gas or liquid regimes and have disregarded possible interactions of one fluid on the other (e.g. Chow and Chung[1]). Representative of the available literature on coupled gas–liquid flows are the investigations of Lock[2] and Kotake,[3] who examined self-similar laminar problems in the absence of pressure gradient, of Schröppel and Thiele,[4] who analysed laminar film condensation on a solid boundary, and those of Street[5] and Liu, Katsaros and Businger,[6] who in simplified analyses considered turbulent transport across an air–water interface.

Accordingly, we present a numerical scheme for solving the two-dimensional, steady-state equations of heat, mass and momentum in a broad class of laminar boundary-layer problems with a smooth, phase-changing, density interface. Both fluid regimes are embedded in a single marching computation which calculates interfacial values of the velocity, shear stress, temperature

*Research Associate.
†Professor of Fluid Mechanics and Applied Mathematics.

0271–2091/85/110957–24$02.40

Received 8 March 1984
Revised 20 May 1985

and mass-transfer rate implicitly as the solution proceeds downstream in the direction of flow. The scheme is an extension of the Box method of Keller and Cebeci,[7] which has been demonstrated to be efficient, accurate and versatile, and which has been used to solve a variety of boundary-layer problems.[8]

Solutions to self-similar and non-similar problems with streamwise pressure-gradient are presented herein. Since self-similar laminar flows are governed by ordinary differential equations, we also include an algorithm for obtaining similarity solutions by Runge–Kutta integration. Some solutions computed by this method are compared to those calculated by the finite-difference scheme in order to assess the accuracy of the latter.

2. BASIC EQUATIONS

In this section we present the non-dimensional equations governing transport of heat, mass, and momentum in laminar gas–liquid flows and discuss the numerical scheme we use to solve them. As illustrated in Figure 1, we consider the forced convection of a constant-property binary mixture of perfect gases flowing over a single-component liquid. The free-stream velocity, temperature, and vapour-concentration in the gaseous regime are denoted by u_∞, T_∞, and m_{v_∞} respectively; $u_{-\infty}$ and $T_{-\infty}$ denote the velocity and temperature in the bulk liquid. (A complete nomenclature is given in Appendix I). Transport of liquid vapour can occur by condensation or evaporation at the interfacial boundary and streamwise pressure gradients above and below the liquid surface may exist. We further assume that the interface remains horizontal (a discussion of this assumption is contained in Appendix II).

2.1. Non-dimensionalization of the coupled boundary-layer problem

The boundary-layer equations we wish to solve are contained in Appendix II. It is convenient, although not absolutely necessary, to non-dimensionalize equations (15)–(17) by introducing a transformation employing the stream function. Let $\psi(x, y)$ be the stream function in physical

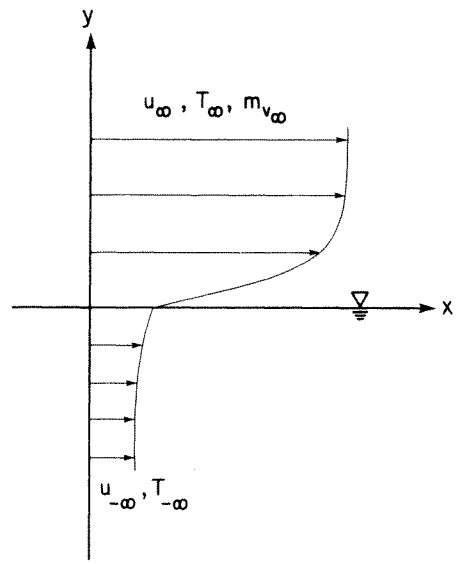

Figure 1. The coupled gas–liquid problem

co-ordinates and $f(\xi, \eta)$ a non-dimensional stream function in the transformed co-ordinate system (ξ, η). If we use the classical Falkner–Skan transformation

$$\psi_1(x, y) = \sqrt{(u_\infty \nu_1 x)} f_1(\xi, \eta_1),$$

$$\psi_2(x, y) = \sqrt{(u_\infty \nu_2 x)} f_2(\xi, \eta_2),$$

$$\eta_1 = \sqrt{\left(\frac{u_\infty}{\nu_1 x}\right)} y_1, \quad \eta_2 = \sqrt{\left(\frac{u_\infty}{\nu_2 x}\right)} y_2, \quad x = \xi$$

and the definition of the stream function given by

$$u_{1,2} = \frac{\partial \psi_{1,2}}{\partial y_{1,2}}, \quad v_{1,2} = -\frac{\partial \psi_{1,2}}{\partial x},$$

the field equations can be written as

$$\frac{\partial^3 f_1}{\partial \eta_1^3} + \frac{m_1 + 1}{2} f_1 \frac{\partial^2 f_1}{\partial \eta_1^2} + m_1 \left[1 - \left(\frac{\partial f_1}{\partial \eta_1}\right)^2\right] = \xi \left(\frac{\partial f_1}{\partial \eta_1} \frac{\partial^2 f_1}{\partial \xi \partial \eta_1} - \frac{\partial f_1}{\partial \xi} \frac{\partial^2 f_1}{\partial \eta_1^2}\right), \tag{1a}$$

$$\frac{1}{Pr_1} \frac{\partial^2 g_1}{\partial \eta_1^2} + \frac{m_1 + 1}{2} f_1 \frac{\partial g_1}{\partial \eta_1}$$

$$+ (d_1 - 1)(Sc^{-1} - Pr_1^{-1})(m_{v_0} - m_{v_\infty}) \frac{\partial}{\partial \eta_1} \left(\frac{g_1}{1 + (d_1 - 1) m_v} \frac{\partial h}{\partial \eta_1}\right) = \xi \left[\frac{\partial f_1}{\partial \eta_1} \frac{\partial g_1}{\partial \xi} - \frac{\partial f_1}{\partial \xi} \frac{\partial g_1}{\partial \eta_1}\right], \tag{1b}$$

$$\frac{1}{Sc} \frac{\partial^2 h}{\partial \eta_1^2} + \frac{m_1 + 1}{2} f_1 \frac{\partial h}{\partial \eta_1} = \xi \left[\frac{\partial f_1}{\partial \eta_1} \frac{\partial h}{\partial \xi} - \frac{\partial f_1}{\partial \xi} \frac{\partial h}{\partial \eta_1}\right], \tag{1c}$$

$$\frac{\partial^2 f_2}{\partial \eta_2^3} + \frac{m_1 + 1}{2} f_2 \frac{\partial^2 f_2}{\partial \eta_2^2} + m_2 \left[\gamma_1^2 - \frac{m_1}{m_2} \left(\frac{\partial f_2}{\partial \eta_2}\right)^2\right] = \xi \left(\frac{\partial f_2}{\partial \eta_2} \frac{\partial^2 f_2}{\partial \xi \partial \eta_2} - \frac{\partial f_2}{\partial \xi} \frac{\partial^2 f}{\partial \eta_2^2}\right), \tag{1d}$$

$$\frac{1}{Pr_2} \frac{\partial^2 g_2}{\partial \eta_2^2} + \frac{m_1 + 1}{2} f_2 \frac{\partial g_2}{\partial \eta_2} = \xi \left[\frac{\partial f_2}{\partial \eta_2} \frac{\partial g_2}{\partial \xi} - \frac{\partial f_2}{\partial \xi} \frac{\partial g_2}{\partial \eta_2}\right], \tag{1e}$$

in which $g_1 = i_1/i_\infty$ and $g_2 = i_2/i_{-\infty}$ are non-dimensional enthalpies, $h = (m_v - m_{v_\infty})/(m_{v_0} - m_{v_\infty})$ is a normalized species-concentration, $m_1 = (\xi/u_\infty)(du_\infty/d\xi)$ and $m_2 = (\xi/u_{-\infty})du_{-\infty}/d\xi$ are the stream-wise pressure-gradient parameters above and below the interface, $\gamma_1 = u_{-\infty}/u_\infty$, and Pr and Sc are the Prandtl and Schmidt numbers, respectively. The underlined term in equation (1b) represents enthalpy transport produced by a species-concentration gradient in the gas.

In stream-function co-ordinates the interfacial and far-field boundary conditions become

$$\left.\frac{\partial f_1}{\partial \eta_1}\right|_0 = \left.\frac{\partial f_2}{\partial \eta_2}\right|_0, \tag{2a}$$

$$\left.\frac{\partial^2 f_1}{\partial \eta_1^2}\right|_0 = \Lambda \left.\frac{\partial^2 f_2}{\partial \eta_2^2}\right|_0, \tag{2b}$$

$$\Lambda \equiv \sqrt{\left(\frac{\rho_2 \mu_2}{\rho_1 \mu_1}\right)},$$

$$g_{1_0} = d_2(1 + (d_1 - 1) m_{v_0})(\gamma_2 g_{2_0} + d_3), \tag{2c}$$

$$d_2 = \frac{C_{p_g}}{C_l}, \quad d_3 = \frac{L_v}{i_\infty}, \quad \gamma_2 = \frac{i_{-\infty}}{i_\infty},$$

$$(m_1+1)f_{1_0}+2\xi\left.\frac{\partial f_1}{\partial\xi}\right|_0=\Lambda\left[(m_1+1)f_{2_0}+2\xi\left.\frac{\partial f_2}{\partial\xi}\right|_0\right], \tag{2d}$$

$$f_{1_0}=\frac{2}{m_1+1}\left[\dot{M}+\xi\left.\frac{\partial f_1}{\partial\xi}\right|_0\right], \quad \dot{M}\equiv\sqrt{\left(\frac{\xi}{\rho_1\mu_1u_\infty}\right)}\dot{m}_0'', \tag{2e}$$

$$\dot{M}=-\frac{(m_{v_0}-m_{v_\infty})}{Sc(1-m_{v_0})}\left.\frac{\partial h}{\partial\eta_1}\right|_0, \tag{2f}$$

$$\dot{M}d_3-\underline{\frac{(d_1-1)(m_{v_0}-m_{v_\infty})}{1+(d_1-1)m_{v_0}}g_{1_0}(Sc^{-1}-Pr_1^{-1})\left.\frac{\partial h}{\partial\eta_1}\right|_0}-\frac{1}{Pr_1}\left.\frac{\partial g_1}{\partial\eta_1}\right|_0+\frac{\gamma_2\Lambda}{Pr_2}\left.\frac{\partial g_2}{\partial\eta_2}\right|_0=0, \tag{2g}$$

$$m_{v_0}=\exp\left[\frac{L_v}{R_v}\left(\frac{1}{T_b}-\frac{1}{T_0}\right)\right], \tag{2h}$$

$$T_0=\frac{i_\infty g_{1_0}}{(1+(d_1-1)m_{v_0})C_{p_g}}, \tag{2i}$$

$$\frac{\partial f_1}{\partial\eta_1}\to 1, \quad g_1\to 1, \quad h\to 0 \quad \text{as} \quad \eta_1\to\infty, \tag{2j}$$

$$\frac{\partial f_2}{\partial\eta_2}\to\gamma_1, \quad g_2\to 1 \quad \text{as} \quad \eta_2\to-\infty. \tag{2k}$$

The underlined term in equation (2g) represents that part of the surface heat flux which results from a vapour-concentration gradient at the interfacial boundary.

2.2. *Numerical solution*

The coupled boundary-layer problem characterized by equations (1) and (2) is parabolic. Solutions of these equations can be obtained in a scheme which commences with input profiles of field quantities at an initial streamwise station and then marches downstream in the direction

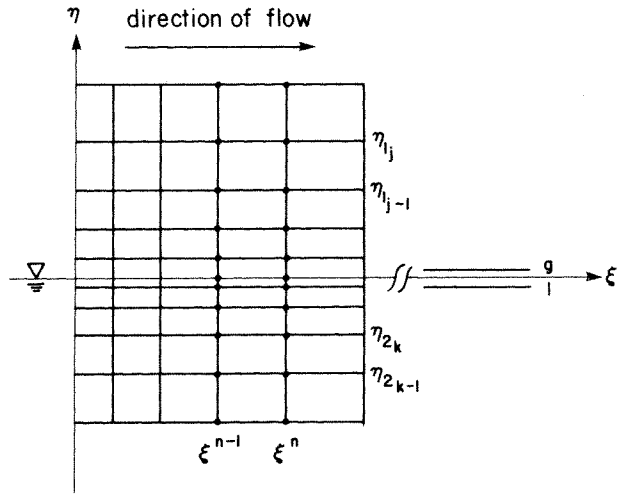

Figure 2. The finite-difference grid for gas–liquid flows

of flow. A typical non-uniform grid over which the finite-difference equations of the Box method are applied is illustrated in Figure 2. A solution is assumed to be known at the streamwise station denoted by ξ^{n-1} and sought at the station ξ^n.

The algorithm we employ for solving equations (1) and (2) appears in Figure 3 and parallels the procedure described by Cebeci and Smith.[8] In this algorithm we exploit the fact that scalar transport affects the transport of momentum only through the single interfacial boundary condition (2e). Consequently, it is possible (and convenient) to solve the momentum equations separately from the remaining equations in the system. The momentum equations are linearized by Newton's method in order to solve them. Once a solution to the momentum problem has been obtained, equation (1c) becomes linear and can be solved directly without recourse to linearization. When solutions to both the momentum and mass transport problems have been obtained, equations (1b) and (1e) become linear and can also be readily solved.

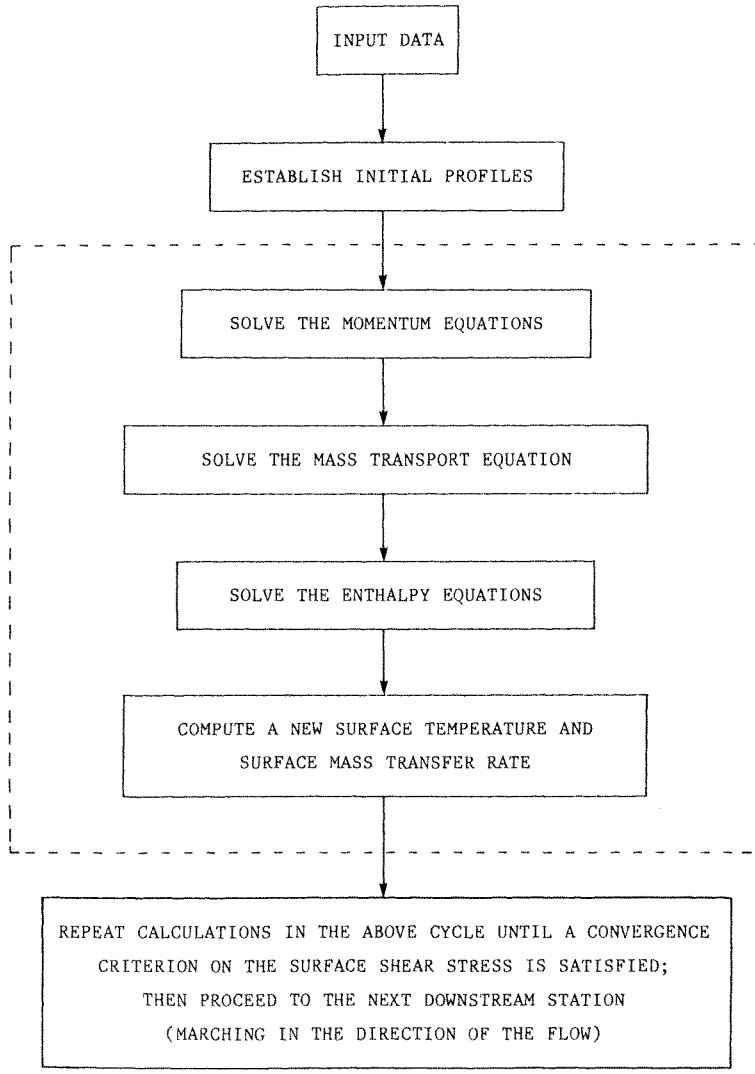

Figure 3. An algorithm for solution of the coupled problem by finite differences

The numerical scheme inherent in the Box method has been described elsewhere.[7-9] In the next sections we discuss those extensions to the method which are required for solving the gas–liquid boundary-layer problem.

2.2.1. Solution of the coupled momentum problem. By introducing new dependent variables $u_1(\xi,\eta_1)$, $v_1(\xi,\eta_1)$, $u_2(\xi,\eta_2)$ and $v_2(\xi,\eta_2)$ we can rewrite equations (1a) and (1d) as a system of first-order partial differential equations; these are given by

$$u_1 = \frac{\partial f_1}{\partial \eta_1}, \tag{3a}$$

$$v_1 = \frac{\partial u_1}{\partial \eta_1}, \tag{3b}$$

$$\frac{\partial v_1}{\partial \eta_1} + \frac{m_1+1}{2} f_1 v_1 + m_1(1-u_1^2) = \xi\left(u_1 \frac{\partial u_1}{\partial \xi} - v_1 \frac{\partial f_1}{\partial \xi}\right), \tag{3c}$$

$$u_2 = \frac{\partial f_2}{\partial \eta_2}, \tag{3d}$$

$$v_2 = \frac{\partial u_2}{\partial \eta_2}, \tag{3e}$$

$$\frac{\partial v_2}{\partial \eta_2} + \frac{m_1+1}{2} f_2 v_2 + m_2\left(\gamma_1^2 - \frac{m_1}{m_2} u_2^2\right) = \xi\left(u_2 \frac{\partial u_2}{\partial \xi} - v_2 \frac{\partial f_2}{\partial \xi}\right). \tag{3f}$$

The interfacial and far-field boundary conditions needed to solve this system are, from (2)

$$u_{1_0} = u_{2_0}, \tag{4a}$$

$$v_{1_0} = \Lambda v_{2_0}, \tag{4b}$$

$$(m_1+1) f_{1_0} + \left.\frac{\partial f_1}{\partial \xi}\right|_0 = \Lambda\left[(m_1+1) f_{2_0} + 2\xi \left.\frac{\partial f_2}{\partial \xi}\right|_0\right], \tag{4c}$$

$$f_{1_0} = -\frac{2}{m_1+1}\left[\dot{M} + 2\xi \left.\frac{\partial f_1}{\partial \xi}\right|_0\right], \tag{4d}$$

$$\lim_{\eta_1 \to \infty} u_1(\xi,\eta_1) = 1, \tag{4e}$$

$$\lim_{\eta_2 \to -\infty} u_2(\xi,\eta_2) = \gamma_1. \tag{4f}$$

Referring to the non-uniform rectangular grid illustrated in Figure 2 we let

$$\xi^0 = 0; \quad \xi^n = \xi^{n-1} + l_n, \quad n = 1,2,\ldots,N, \tag{5a}$$

$$\eta_{1_0} = 0; \quad \eta_{1_j} = \eta_{1_{j-1}} + p_{1_j}, \quad j = 1,2,\ldots,J, \tag{5b}$$

$$\eta_{2_0} = 0; \quad \eta_{2_k} = \eta_{2_{k+1}} - p_{2_k}, \quad k = -1,-2,\ldots,-K \tag{5c}$$

denote the net spacings, and adopt the customary notation

$$\xi^{n-1/2} = \tfrac{1}{2}(\xi^n + \xi^{n-1}), \tag{5d}$$

$$\eta_{1_{j-1/2}} = \tfrac{1}{2}(\eta_{1_j} + \eta_{1_{j-1}}); \quad \eta_{2_{k+1/2}} = \tfrac{1}{2}(\eta_{2_{k+1}} + \eta_{2_k}) \tag{5e}$$

for points centred between net points in the grid. Furthermore, we approximate the unknowns (f_1^n, u_1^n, v_1^n) at (ξ^n, η_{1_j}) and (f_2^n, u_2^n, v_2^n) at (ξ^n, η_{2_k}) by the respective net functions $(f_{1_j}^n, u_{1_j}^n, v_{1_j}^n)$ and $(f_{2_k}^n, u_{2_k}^n, v_{2_k}^n)$ in the usual manner, and let

$$q_\alpha^{n-1/2} = \tfrac{1}{2}(q_\alpha^n + q_\alpha^{n-1}), \quad q_{\alpha-1/2}^n = \tfrac{1}{2}(q_\alpha^n + q_{\alpha-1}^n) \tag{5f}$$

for any net function $q_\alpha^n (\alpha = j, k+1)$ above or below the interface.

The centred-difference approximations to (3a), (3b), (3d) and (3e) are simple. However, since (3c) and (3f) contain derivatives with respect to variables in two orthogonal directions, the process of differencing these equations must be accomplished in two steps. Details of this procedure are contained elsewhere[8-10] and are omitted here. The finite-difference approximations to equations (3) are given by

$$u_{1_{j-1/2}}^n = (f_{1_j}^n - f_{1_{j-1}}^n)/p_{1_j}, \tag{6a}$$

$$v_{1_{j-1/2}}^n = (u_{1_j}^n - u_{1_{j-1}}^n)/p_{1_j}, \tag{6b}$$

$$\begin{aligned}(v_{1_j}^n - v_{1_{j-1}}^n)/p_{1_j} + (\tfrac{1}{2})(2\alpha_n + m_1^n + 1)(f_1 v_1)_{j-1/2}^n - (\alpha_n + m_1^n)(u_1^2)_{j-1/2}^n \\ + \alpha_n(f_{1_{j-1/2}}^n v_{1_{j-1/2}}^{n-1} - f_{1_{j-1/2}}^{n-1} v_{1_{j-1/2}}^n) = R_{1_{j-1/2}}^{n-1},\end{aligned} \tag{6c}$$

$$u_{2_{k+1/2}}^n = (f_{2_{k+1}}^n - f_{2_k}^n)/p_{2_k}, \tag{6d}$$

$$v_{2_{k+1/2}}^n = (u_{2_{k+1}}^n - u_{2_k}^n)/p_{2_k}, \tag{6e}$$

$$\begin{aligned}(v_{2_{k+1}}^n - v_{2_k}^n)/p_{2_k} + (\tfrac{1}{2})(2\alpha_n + m_1^n + 1)(f_2 v_2)_{k+1/2}^n - (\alpha_n + m_1^n)(u_2^2)_{k+1/2}^n \\ + \alpha_n(f_{2_{k+1/2}}^n v_{2_{k+1/2}}^{n-1} - f_{2_{k+1/2}}^{n-1} v_{2_{k+1/2}}^n) = R_{2_{k+1/2}}^{n-1},\end{aligned} \tag{6f}$$

in which

$$\begin{aligned}R_{1_{j-1/2}}^{n-1} = -[(v_{1_j} - v_{1_{j-1}})/p_{1_j} + (\tfrac{1}{2})(m_1 + 1 - 2\alpha_n)(f_1 v_1)_{j-1/2} \\ + (\alpha_n - m_1)(u_1^2)_{j-1/2} + m_1]^{n-1} - m_1^n\end{aligned}$$

and

$$\begin{aligned}R_{2_{k+1/2}}^{n-1} = -[(v_{2_{k+1}} - v_{2_k})/p_{2_k} + (\tfrac{1}{2})(m_1 + 1 - 2\alpha_n)(f_2 v_2)_{k+1/2} \\ + (\alpha_n - m_1)(u_2^2)_{k+1/2} + m_2\gamma_1^2]^{n-1} - (m_2\gamma_1^2)^n\end{aligned}$$

contain elements of the solution at ξ^{n-1} and where $\alpha_n = \xi^{n-1/2}/l_n$, $j = 1, 2, \ldots, J$ and $k = -1, \ldots, -K$.

The difference approximations to the interfacial and far-field boundary conditions are given by

$$u_{1_0}^n = u_{2_0}^n, \tag{7a}$$

$$v_{1_0}^n = \Lambda v_{2_0}^n, \tag{7b}$$

$$(m_1^n + 1 + 4\alpha_n)(f_{1_0}^n - \Lambda f_{2_0}^n) = -(m_1^{n-1} + 1 - 4\alpha_n)(f_{1_0}^{n-1} - \Lambda f_{2_0}^{n-1}), \tag{7c}$$

$$(m_1^n + 1 + 4\alpha_n) f_{1_0}^n = -2(\dot{M}^n + \dot{M}^{n-1}) - (m_1^{n-1} + 1 - 4\alpha_n) f_{1_0}^{n-1}, \tag{7d}$$

$$u_{1_j}^n = 1, \tag{7e}$$

$$u_{2_{-K}}^n = \gamma_1. \tag{7f}$$

The far-field boundary conditions (7e) and (7f) are enforced at the respective ordinates denoted by η_{1_J} and $\eta_{2_{-K}}$, which are assumed to be sufficiently large that the asymptotic limits implied by (2j) and (2k) are satisfied.

Equations (6) and (7) comprise a non-linear system of $3J + 3K + 6$ difference equations at ξ^n in the rectangular grid depicted in Figure 2; a solution is, of course, known at ξ^{n-1}. Newton's method is employed to linearize this system in order to solve it. We adopt the notation of Keller[10] and introduce the iterates $(f_{1_j}^{n,i}, u_{1_j}^{n,i}, v_{1_j}^{n,i})$ and $(f_{2_k}^{n,i}, u_{2_k}^{n,i}, v_{2_k}^{n,i})$ of the unknowns for the ith iteration

$(i = 0, 1, \ldots)$ at ξ^n. If

$$f_{1_j}^{n,i+1} = f_{1_j}^{n,i} + \delta f_{1_j}, \quad u_{1_j}^{n,i+1} = u_{1_j}^{n,i} + \delta u_{1_j},$$
$$v_{1_j}^{n,i+1} = v_{1_j}^{n,i} + \delta v_{1_j}, \quad j = 0, 1, \ldots, J, \tag{8a}$$

and

$$f_{2_k}^{n,i+1} = f_{2_k}^{n,i} + \delta f_{2_k}, \quad u_{2_k}^{n,i+1} = u_{2_k}^{n,i} + \delta u_{2_k},$$
$$v_{2_k}^{n,i+1} = v_{2_k}^{n,i} + \delta v_{2_k}, \quad k = 0, -1, \ldots, -K, \tag{8b}$$

then by substituting (8) into (6) and (7) and retaining terms which are first-order in the δ-iterates we obtain the following set of linearized matrix equations:

$$\begin{aligned}
&\mathbf{B}_{1_j}\delta_{1_{j-1}} + \mathbf{A}_{1_j}\boldsymbol{\delta}_{1_j} = \mathbf{r}_{1_j},\\
&\mathbf{B}_{1_j}\boldsymbol{\delta}_{1_{j-1}} + \mathbf{A}_{1_j}\boldsymbol{\delta}_{1_j} + \mathbf{C}_{1_j}\boldsymbol{\delta}_{1_{j+1}} = \mathbf{r}_{1_j}, \quad 1 \leqslant j \leqslant J-1,\\
&\mathbf{B}_{1_0}\boldsymbol{\delta}_{2_0} + \mathbf{A}_{1_0}\boldsymbol{\delta}_{1_0} + \mathbf{C}_{1_0}\boldsymbol{\delta}_{1_1} = \mathbf{r}_{1_0},\\
&\mathbf{C}_{2_0}\boldsymbol{\delta}_{2_{-1}} + \mathbf{A}_{2_0}\boldsymbol{\delta}_{2_0} + \mathbf{B}_{2_0}\boldsymbol{\delta}_{1_0} = \mathbf{r}_{2_0},\\
&\mathbf{C}_{2_k}\boldsymbol{\delta}_{2_{k-1}} + \mathbf{A}_{2_k}\boldsymbol{\delta}_{2_k} + \mathbf{B}_{2_k}\boldsymbol{\delta}_{2_{k+1}} = \mathbf{r}_{2_k}, \quad -K+1 \leqslant k \leqslant -1,\\
&\mathbf{A}_{2_{-K}}\boldsymbol{\delta}_{2_{-K}} + \mathbf{B}_{2_{-K}}\boldsymbol{\delta}_{2_{-K+1}} = \mathbf{r}_{2_{-K}},
\end{aligned} \tag{9}$$

in which $\boldsymbol{\delta}_{1_j} = [\delta f_{1_j}, \delta u_{1_j}, \delta v_{1_j}]^{\mathrm{T}}$ and $\boldsymbol{\delta}_{2_k} = [\delta f_{2_k}, \delta u_{2_k}, \delta v_{2_k}]^{\mathrm{T}}$ are vectors of the unknowns at points (n,j) and (n,k), respectively, for the $(i+1)$th iteration, $\mathbf{r}_{1_j}$ and $\mathbf{r}_{2_k}$ are vectors containing difference approximations of field variables at ξ^n and ξ^{n-1} and $\mathbf{A}_{1_j}$, $\mathbf{B}_{1_j}$, $\mathbf{C}_{1_j}$, $\mathbf{A}_{2_k}$, $\mathbf{B}_{2_k}$, and $\mathbf{C}_{2_k}$ are 3×3 matrices whose elements are defined by Klotz and Street.[11]

The unique nature of the interfacial coupling and the precise structure of the difference equations become more apparent if we rewrite the system of matrix equations (9) in block tridiagonal form,

$$\mathbf{P}\boldsymbol{\delta} = \mathbf{r}, \tag{10}$$

where

$$\boldsymbol{\delta} = \begin{bmatrix} \boldsymbol{\delta}_{2_{-K}} \\ \boldsymbol{\delta}_{2_{-K+1}} \\ \vdots \\ \boldsymbol{\delta}_{2_0} \\ \boldsymbol{\delta}_{1_0} \\ \vdots \\ \boldsymbol{\delta}_{1_{J-1}} \\ \boldsymbol{\delta}_{1_J} \end{bmatrix}, \quad \mathbf{r} = \begin{bmatrix} \mathbf{r}_{2_{-K}} \\ \mathbf{r}_{2_{-K+1}} \\ \vdots \\ \mathbf{r}_{2_0} \\ \mathbf{r}_{1_0} \\ \vdots \\ \mathbf{r}_{1_{J-1}} \\ \mathbf{r}_{1_J} \end{bmatrix}$$

and

$$\mathbf{P} = \begin{bmatrix}
\mathbf{A}_{2_{-K}} & \mathbf{B}_{2_{-K}} & & & & & & & & & \\
\mathbf{C}_{2_{K+1}} & \mathbf{A}_{2_{-K+1}} & \mathbf{B}_{2_{-K+1}} & & & & & & & & \\
 & \ddots & \ddots & \ddots & & & & & & & \\
 & & \ddots & \ddots & \ddots & & & & & & \\
 & & & \mathbf{C}_{2_{-1}} & \mathbf{A}_{2_{-1}} & \mathbf{B}_{2_{-1}} & & & & & \\
 & & & & \mathbf{C}_{2_0} & \mathbf{A}_{2_0} & \mathbf{B}_{2_0} & & & & \\
 & & & & & \mathbf{B}_{1_0} & \mathbf{A}_{1_0} & \mathbf{C}_{1_0} & & & \\
 & & & & & & \mathbf{B}_{1_1} & \mathbf{A}_{1_1} & \mathbf{C}_{1_1} & & \\
 & & & & & & & \ddots & \ddots & \ddots & \\
 & & & & & & & & \ddots & \ddots & \ddots \\
 & & & & & & & & \mathbf{B}_{1_{J-1}} & \mathbf{A}_{1_{J-1}} & \mathbf{C}_{1_{J-1}} \\
 & & & & & & & & & \mathbf{B}_{1_J} & \mathbf{C}_{1_J}
\end{bmatrix},$$

As is evident, the interfacial boundary conditions are embedded in the structure of the coefficient matrix **P**. Consequently, the simplicity and efficiency inherent in the box method is maintained and, since the difference equations at each streamwise station are implicit, the quadratic convergence characteristic of Newton's method is preserved.

In order to solve (10) we adopt the block elimination procedure described by Isaacson and Keller[12] and Keller.[13] Details of the method, which has been applied to boundary-layer problems over solid surfaces, are contained in Reference 9 and are not repeated here.

2.2.2. Solution of the coupled enthalpy and mass transport problems. The differential equations and boundary conditions characterizing the transport of scalar quantities can be readily solved without recourse to linearization using Newton's method. The systems of differenced scalar equations also possess a structure less complex than the corresponding system for momentum.

To solve the enthalpy problem we introduce new dependent variables $G_1(\xi, \eta_1)$ and $G_2(\xi, \eta_2)$ and rewrite equations (1b) and (1e) as a system of first-order partial differential equations, namely

$$G_1 = \frac{\partial g_1}{\partial \eta_1}, \tag{11a}$$

$$\frac{1}{Pr_1}\frac{\partial G_1}{\partial \eta_1} + \frac{m_1 + 1}{2} f_1 G_1 + D_1 \frac{\partial}{\partial \eta_1}(D_2 g_1) = \xi\left[u_1 \frac{\partial g_1}{\partial \xi} - G_1 \frac{\partial f_1}{\partial \xi}\right], \tag{11b}$$

$$G_2 = \frac{\partial g_2}{\partial \eta_2}, \tag{11c}$$

$$\frac{1}{Pr_2}\frac{\partial G_2}{\partial \eta_2} + \frac{m_1 + 1}{2} f_2 G_2 = \xi\left[u_2 \frac{\partial g_2}{\partial \xi} - G_2 \frac{\partial f_2}{\partial \xi}\right], \tag{11d}$$

in which $H = \partial h/\partial \eta_1$, $D_1 = (d_1 - 1)(Sc^{-1} - Pr_1^{-1})(m_{v_0} - m_{v_\infty})$ and $D_2 = H/[1 + (d_1 - 1)m_v]^{-1}$. From (2) the interfacial and far-field boundary conditions for the enthalpy problem become

$$g_{1_0} - [1 + (d_1 - 1)m_{v_0}]d_2(\gamma_2 g_{2_0} + d_3) = 0, \tag{12a}$$

$$\dot{M} d_3 - D_1 D_{2_0} g_{1_0} - \frac{1}{Pr_1} G_{1_0} + \frac{\Lambda \gamma_2}{Pr_2} G_{2_0} = 0, \tag{12b}$$

$$\lim_{\eta_1 \to \infty} g_1(\xi, \eta_1) = 1, \tag{12c}$$

$$\lim_{\eta_2 \to -\infty} g_2(\xi, \eta_2) = 1. \tag{12d}$$

Equations (11) and (12) are linear in the dependent variables when solutions to the momentum and mass transport problems have been computed.

If $\boldsymbol{\delta}_{e1_j} = [g^n_{1_j}, G^n_{1_j}]^T$ and $\boldsymbol{\delta}_{e2_k} = [g^n_{2_k}, G^n_{2_k}]^T$ are vectors of the unknowns at the vertical grid points (n, j) and (n, k), respectively, the system of difference equations governing enthalpy transport can be written as

$$\begin{aligned}
&\mathbf{B}_{e1_J}\boldsymbol{\delta}_{e1_{J-1}} + \mathbf{A}_{e1_J}\boldsymbol{\delta}_{e1_J} = \mathbf{r}_{e1_J},\\
&\mathbf{B}_{e1_j}\boldsymbol{\delta}_{e1_{j-1}} + \mathbf{A}_{e1_j}\boldsymbol{\delta}_{e1_j} + \mathbf{C}_{e1_j}\boldsymbol{\delta}_{e1_{j+1}} = \mathbf{r}_{e1_j}, \quad 1 \leqslant j \leqslant J-1,\\
&\mathbf{B}_{e1_0}\boldsymbol{\delta}_{e2_0} + \mathbf{A}_{e1_0}\boldsymbol{\delta}_{e1_0} + \mathbf{C}_{e1_0}\boldsymbol{\delta}_{e1_1} = \mathbf{r}_{e1_0},\\
&\mathbf{C}_{e2_0}\boldsymbol{\delta}_{e2_{-1}} + \mathbf{A}_{e2_0}\boldsymbol{\delta}_{e2_0} + \mathbf{B}_{e2_0}\boldsymbol{\delta}_{e1_0} = \mathbf{r}_{e2_0},\\
&\mathbf{C}_{e2_k}\boldsymbol{\delta}_{e2_{k-1}} + \mathbf{A}_{e2_k}\boldsymbol{\delta}_{e2_k} + \mathbf{B}_{e2_k}\boldsymbol{\delta}_{e2_{k+1}} = \mathbf{r}_{e2_k}, \quad -K+1 \leqslant k \leqslant -1,\\
&\mathbf{A}_{e2_{-K}}\boldsymbol{\delta}_{e2_{-K}} + \mathbf{B}_{e2_{-K}}\boldsymbol{\delta}_{e2_{-K+1}} = \mathbf{r}_{e2_{-K}}
\end{aligned} \tag{13}$$

in which $\mathbf{r}_{e1_j}$ and $\mathbf{r}_{e2_k}$ are vectors containing finite-difference approximations of variables at ξ^n and ξ^{n-1} and $\mathbf{A}_{e1_j}$, $\mathbf{B}_{e1_j}$, $\mathbf{C}_{e1_j}$, $\mathbf{A}_{e2_k}$, $\mathbf{B}_{e2_k}$ and $\mathbf{C}_{e2_k}$ are 2×2 matrices whose elements are defined by Klotz and Street.[11] To solve equations (13) we rewrite them in block tridiagonal form and adopt the elimination method described in Section 2.2.1. The procedure is straightforward and we therefore omit the details of it.

Equation (1c), subject to boundary conditions given by

$$h_0 = 1,$$
$$\lim_{\eta_1 \to \infty} h = 0,$$

can be readily solved using the same elimination scheme. Accomplishing this task only requires minor modification of the block tridiagonal matrix which corresponds to equations (13).

2.3. *The generation of initial profiles and convergence criteria for the coupled gas–liquid problem*

Any one of a variety of methods can be employed to provide initial distributions of dependent variables at the first streamwise station in the flow field. We may, for example, use experimental data to start calculations, but if data is not available it is possible to initialize computations by calculating a self-similar solution to equations (1) and (2). In the latter case we locate the first station at $\xi = 0$ and let

$$f_1 = a_{11}\eta_1 + (\tfrac{1}{2})a_{12}\eta_1^2 + (\tfrac{1}{4})a_{13}\eta_1^4,$$
$$f_2 = a_{21}\eta_2 + (\tfrac{1}{2})a_{22}\eta_2^2 + (\tfrac{1}{4})a_{23}\eta_2^4, \tag{14}$$

be the initial approximation to the stream functions above and below the interfacial boundary, where

$$a_{11} = a_{21} = 1 + \frac{(1-\gamma_1)\eta_\infty}{\Lambda^{-1}\eta_{-\infty} - \eta_\infty},$$

$$a_{12} = -\frac{3(1-\gamma_1)}{2(\Lambda^{-1}\eta_{-\infty} - \eta_\infty)}, \quad a_{22} = \Lambda^{-1}a_{12},$$

$$a_{13} = \frac{1-\gamma_1}{2\eta_\infty^2(\Lambda^{-1}\eta_{-\infty} - \eta_\infty)}, \quad a_{23} = \frac{a_{21} - \gamma_1}{2\eta_{-\infty}^3}.$$

By using this approximation we are able to start calculations without specifying initial distributions of scalar variables. Profiles of f_1', f_1'', f_2' and f_2'' across the boundary layers are needed, however, and are easily obtained by differentiating the functions in (14), which satisfy the boundary conditions

$$f_{1_\infty}' = 1, \quad f_{1_\infty}'' = 0,$$
$$f_{2_{-\infty}}' = \gamma_1, \quad f_{2_{-\infty}}'' = 0,$$
$$f_{1_0} = f_{2_0} = 0, \quad f_{1_0}' = f_{2_0}', \quad f_{1_0}'' = \Lambda f_{2_0}''.$$

Calculations at each streamwise station are terminated only when a convergence criterion on the interfacial shear stress is satisfied. This criterion is given by $|\delta v_{1_0}| \leqslant \varepsilon$, where $\varepsilon \sim O(10^{-5})$ is a prescribed tolerance parameter. Additional criteria on the surface drift, interfacial temperature, and mass transfer rate are usually not warranted.

Self-similar problems which use equations (14) as an initial approximation generally require no more than 10–20 iterations before a converged solution is obtained, even for flows with strong

surface evaporation or condensation. In non-similar problems, which we can solve by marching downstream from the self-similar solution at $\xi = 0$, if the horizontal grid spacing is constant (or nearly so), the number of iterations required for convergence at a particular station usually decreases as ξ increases, unless an adverse pressure gradient is present and computations are being performed near a separation point, or the grid spacing is so large that the solution changes markedly between adjacent stations. In either case, in order to compute an accurate solution we must refine the horizontal grid and repeat all calculations.

In many boundary-layer flows streamlines are essentially parallel to lines of constant η and boundary-layer growth in physical co-ordinates is automatically accounted for in the transformed (ξ, η) co-ordinate system. However, in some problems (i.e. those with pressure gradient), the vertical grid at downstream stations must be expanded in one or the other fluid regime to ensure that the boundary layers are contained entirely within the computational domain. Our finite-difference algorithm requires that $|v_{1_J}| \leqslant \lambda_1$ and $|v_{2_{-K}}| \leqslant \lambda_2$ at each streamwise station in the flow field, where λ_1 and λ_2 are tolerance parameters, $O(10^{-3})$ and $O(10^{-4})$, respectively. If either of these criteria is not satisfied at any station, additional points are added to the vertical grid in one or the other fluid regime and the iteration process described above repeated until the convergence criterion on $|\delta v_{1_0}|$ is also satisfied. The details of this procedure have been described by Cebeci and Bradshaw.[9]

3. RESULTS

In Appendix III we compare self-similar solutions calculated by the scheme described above to those computed by Runge–Kutta integration. In this section we present the results of additional finite-difference computations. Unlike the results presented in Appendix III, however, those which we discuss here were obtained by retaining the underlined mass transport terms in equations (1b) and (2g).

In all our finite-difference calculations we used the particular computational grid suggested by Cebeci and Bradshaw.[9] We specified horizontal grid spacing arbitrarily, defined vertical grid point locations by

$$\eta_{1_j} = \eta_{1_1} \frac{S_1^j - 1}{S_1 - 1}, \qquad S_1 \geqslant 1; j = 1, 2, \ldots, J,$$

in the gas and

$$\eta_{2_k} = \eta_{2_{-1}} \frac{S_2^{-k} - 1}{S_2 - 1}, \quad S_2 \geqslant 1; k = -1, -2, \ldots, -K,$$

in the liquid, and calculated the number of node points above and below the interfacial boundary from expressions given, respectively, by,

$$J = \frac{\ln(1 + (S_1 - 1)\eta_\infty/\eta_{1_1})}{\ln S_1},$$

and

$$K = \frac{\ln(1 + (S_2 - 1)\eta_{-\infty}/\eta_{2_{-1}})}{\ln S_2}$$

where S_1 and S_2 are constant ratios of adjacent grid intervals. In our computations $1{\cdot}02 \leqslant S_1 \leqslant 1{\cdot}05$, $1{\cdot}05 \leqslant S_2 \leqslant 1{\cdot}1$, $0{\cdot}05 \leqslant \eta_{1_1} \leqslant 0{\cdot}10$, $-0{\cdot}10 \leqslant \eta_{2_1} \leqslant -0{\cdot}2$, $8 \leqslant \eta_\infty \leqslant 11$ and $-24 \leqslant \eta_{-\infty} \leqslant -128$. Actual values used in a particular simulation depended on the magnitude

of the pressure-gradient parameters m_1 and m_2, mean current to free-stream velocity ratio γ_1, and surface mass transfer rate $\dot{M}$. We also imposed a maximum value of 5 on p_{2_k} below the interfacial boundary because node spacings in the subsurface regime may become large with the magnitudes of S_2, η_{2_1}, and $\eta_{-\infty}$ cited above.

Self-similar solutions of equations (1) and (2) exist if all dependent variables are independent of the streamwise co-ordinate ξ, if m_1, γ_1, and γ_2 are constants, and if either (a) $m_2 = m_1$ when $\gamma_1 \neq 0$ or (b) $\gamma_1 = 0$. We computed such solutions to a number of problems involving the air–water system under different bulk fluid conditions and plotted calculated values of the shear stress $f''_{1_0} = d^2 f_1/d\eta_1^2|_0$, heat transfer coefficient $-\theta'_{1_0} = (T_\infty - T_0)^{-1} dT_1/d\eta_1|_0$, and mass transfer rate $\dot{M}$ in Figures 4–7. In each simulation $T_\infty = 100\,^\circ\text{C}$. All properties were obtained from Reference 14 and evaluated at the corresponding far-field temperature. Of particular importance to this discussion are effects of mild pressure gradient and a mean current in the liquid on interfacial parameters under conditions of both condensation ($\dot{M} < 0$) and evaporation ($\dot{M} > 0$).

Figure 4 indicates that a favourable pressure gradient ($m_1 > 0$) increases f''_{1_0}, $-\theta'_{1_0}$ and $\dot{M}$ from the values one obtains when no pressure gradient exists; an unfavourable pressure gradient ($m_1 < 0$) clearly has an opposite effect. The heat transfer coefficient $-\theta'_{1_0}$ is obviously affected by pressure gradient to a lesser extent than is the interfacial shear stress. This result is not surprising because there is no term in equation (1b) which is analogous to the pressure-gradient term in (1a).

Figure 5 illustrates effects of a liquid current on several interfacial parameters in the absence of pressure gradient and free-stream humidity. In these cases the liquid surface is evaporating. An

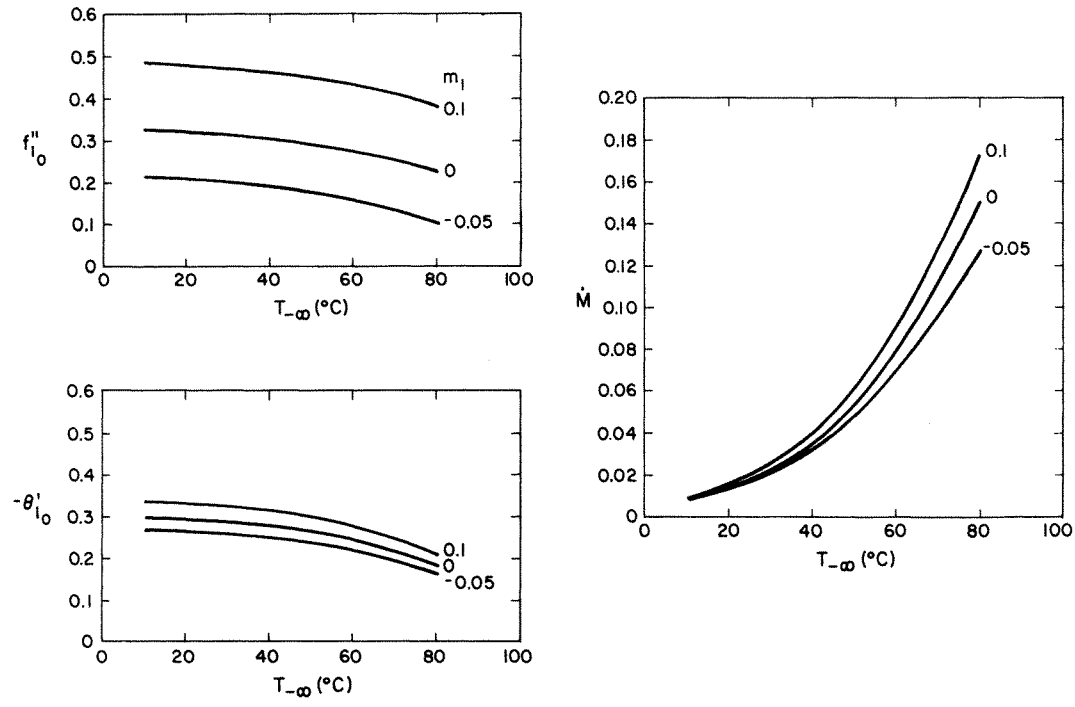

Figure 4. Effect of mild pressure-gradient on interfacial parameters in laminar, gas–liquid flows (air–water system; $T_\infty = 100\,^\circ\text{C}$, $\gamma_1 = m_{v_\infty} = 0$). In this Figure f''_{1_0}, $-\theta'_{1_0}$ and $\dot{M}$ are the interfacial shear stress, heat transfer coefficient and mass transfer rate, respectively, and m_1 is the pressure-gradient parameter in the gaseous regime

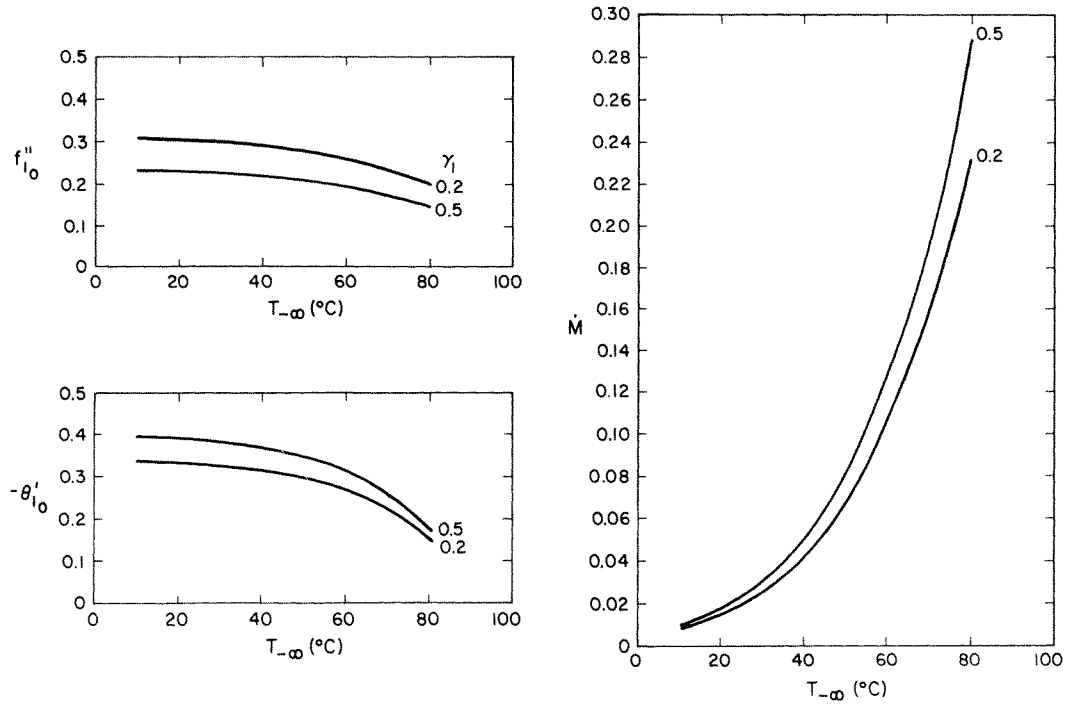

Figure 5. Effect of liquid current on interfacial parameters in laminar, gas–liquid flows (air–water system; $T_\infty = 100\,°C$, $m_1 = m_{v_\infty} = 0$). In this Figure $\gamma_1 = u_{-\infty}/u_\infty$; all remaining symbols are the same as in Figure 4

increasing current decreases the shear stress but increases the heat transfer coefficient and surface mass transfer rate at all temperatures. A mean current beneath the interfacial boundary dramatically thins the boundary layers in the subsurface regime. Consequently, a higher surface temperature results with a subsequent increase in the mass transfer rate.

Figure 6 illustrates effects of a variable free-stream concentration of water vapour on interfacial parameters in the absence of pressure gradient and mean current. An increase in m_{v_∞} results in an increase in the surface shear stress and heat transfer coefficients, but a decrease in the mass transfer rate. When condensation occurs, water vapour is transported through the boundary layer from the free stream to the surface where it undergoes phase change and releases its latent heat. Since latent heat is a large quantity in the energy budget at the interface, a higher surface temperature results when condensing fluid is deposited there. As the condensation rate increases, the boundary layers above the interface become progressively thinner and the skin friction and heat transfer coefficients increase further.

Figure 7 depicts the combined effects of condensation and a mild favorable pressure gradient on f''_{1_0}, $-\theta'_{1_0}$ and $\dot{M}$. Not surprisingly, the effect of an increasing rate of condensation is accentuated by a favourable pressure gradient and the surface shear stress and heat transfer coefficient increase for all temperatures when $m_1 > 0$.

These results correct and extend those reported by Kotake,[3] who considered self-similar gas–liquid problems in the absence of pressure gradient and mean current. In contrast to Kotake's erroneous results, our calculations indicate that when the mass transfer rate is sufficiently large, the surface temperature may be markedly depressed below the fluid temperatures far above and below the interface (Table I). This result is not surprising when one recognizes that $\dot{M}$ is primarily

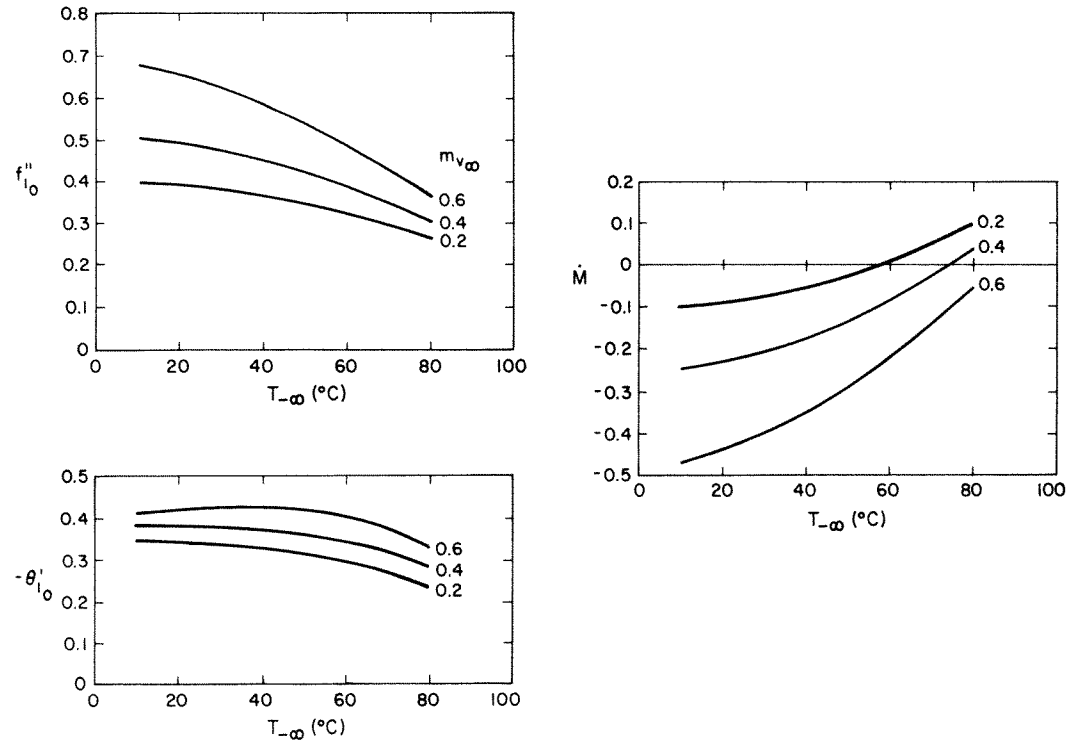

Figure 6. Effect of free-stream vapour concentration on interfacial parameters in laminar gas–liquid flows (air–water system; $T_\infty = 100\,°C$, $m_1 = \gamma_1 = 0$). In this Figure m_{v_∞} is the free-stream vapour concentration in the gas. All remaining symbols are the same as in Figure 4

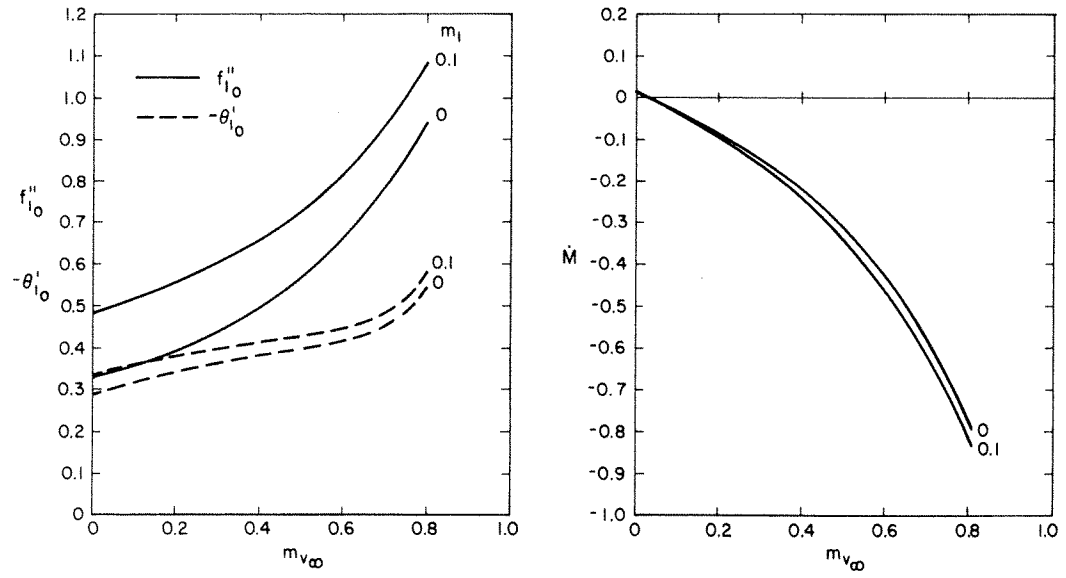

Figure 7. Combined effects of condensation and mild favourable pressure-gradient on interfacial parameters in laminar, gas–liquid flows (air–water system; $T_\infty = 100\,°C$, $\gamma_1 = 0$). All symbols are the same as in Figures 4–6

Table I. Surface temperatures for several self-similar, laminar flows (air–water system; $\gamma_1 = m_1 = 0$)

T_∞(°C)	$T_{-\infty}$(°C)	m_{v_∞}	$\dot{M}$	T_0(°C)
100	20	0	0·013	20·1
		0·2	−0·088	28·4
		0·4	−0·288	38·6
	50	0	0·054	46·5
	80	0	0·150	68·2
		0·2	0·147	75·4
20	20	0	0·009	19·2

controlled by the bulk liquid temperature and free-stream vapour concentration, and that evaporating fluid absorbs its latent heat when it undergoes phase change.

Finally, we present the results of two non-similar boundary-layer calculations in which surface evaporation occurs. One simulation is of a linearly accelerating flow in which $u_\infty = 1 + \xi$; the other is of a linearly retarded (Howarth) flow in which $u_\infty = 1 - \xi$. In each $T_\infty = 100\,°C$, $T_{-\infty} = 80\,°C$, $m_{v_\infty} = 0$ and $\gamma_1 = 0$. Both simulations were started from the same self-similar solution at $\xi = 0$ and computed on progressively finer horizontal and vertical grids until accurate solutions were obtained. Horizontal grid spacing decreased with distance from $\xi = 0$ in the retarded flow, but increased with distance in the flow with favorable pressure gradient. The streamwise grid point

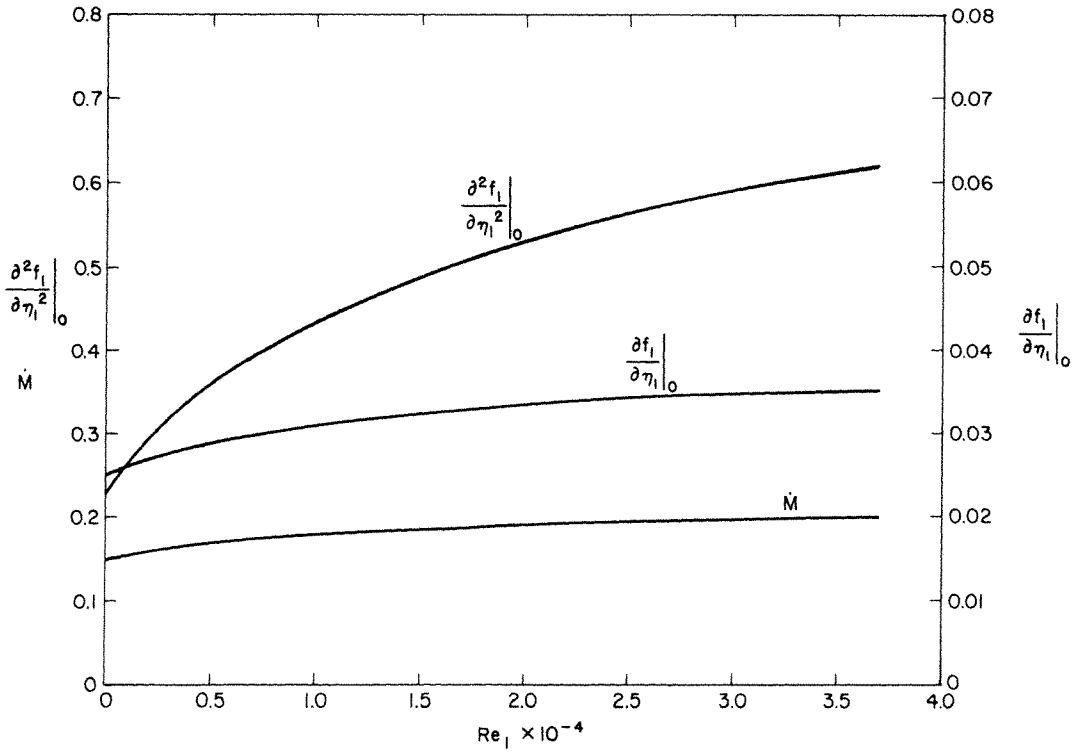

Figure 8. Interfacial parameters in an accelerating laminar flow ($u_\infty = 1 + \xi$, $T_\infty = 100\,°C$, $T_{-\infty} = 80\,°C$, $m_{v_\infty} = \gamma_1 = 0$). In this Figure $\partial f_1/\partial \eta_1|_0$, $\partial^2 f_2/\partial \eta_2^2|_0$ and $\dot{M}$ denote the velocity, shear stress and mass transfer rate at the interfacial boundary

Table II. Computational parameters and horizontal grid point locations for two non-similar flows (air–water system)*

Decelerating flow: $u_\infty = 1 - \xi$		Accelerating flow: $u_\infty = 1 + \xi$	
$S_1 = 1{\cdot}02$,	$S_2 = 1{\cdot}05$	$S_1 = 1{\cdot}02$,	$S_2 = 1{\cdot}05$
$\eta_{1_1} = 0{\cdot}1$,	$\eta_{2_{-1}} = -0{\cdot}2$	$\eta_{1_1} = 0{\cdot}1$,	$\eta_{2_{-1}} = -0{\cdot}2$
$\eta_\infty = 11$,	$\eta_{-\infty} = -96$	$\eta_\infty = 10$,	$\eta_{-\infty} = -90$
Station	ξ	Station	ξ
1	0·0000	1	0·00
2	0·0050	2	0·01
3	0·0100	3	0·02
4	0·0150	4	0·03
5	0·0200	5	0·04
6	0·0250	6	0·05
7	0·0300	7	0·06
8	0·0350	8	0·07
9	0·0400	9	0·08
10	0·0450	10	0·09
11	0·0500	11	0·10
12	0·0550	12	0·12
13	0·0600	13	0·14
14	0·0650	14	0·16
15	0·0700	15	0·18
16	0·0740	16	0·20
17	0·0780	17	0·22
18	0·0810	18	0·25
19	0·0840	19	0·28
20	0·0860	20	0·31
21	0·0880	21	0·34
22	0·0900	22	0·38
23	0·0910	23	0·42
24	0·0920	24	0·46
25	0·0930	25	0·50
26	0·0935	26	0·55
27	0·0940		
28	0·0942		
29	0·0944		
30	0·0946		
31	0·0947		
32	0·0948		
33	0·0949		
34	0·0950		

*In each $T_\infty = 100\,^\circ\text{C}$, $T_{-\infty} = 80\,^\circ\text{C}$, $m_{v_\infty} = 0$ and $\gamma_1 = 0$.

locations and values of S_1, η_{1_1}, η_∞, S_2, $\eta_{2_{-1}}$ and $\eta_{-\infty}$ which are recorded in Table II resulted in surface parameters everywhere accurate to three significant figures.

The interfacial velocity, shear stress and surface mass transfer rate in these flows are plotted as functions of Reynolds number in Figures 8 and 9. Calculations in the accelerating flow were arbitrarily terminated at $\xi = 0{\cdot}55$ ($Re_1 \simeq 3{\cdot}7 \times 10^4$). In the retarded flow boundary-layer separation occurred at $\xi \simeq 0{\cdot}095$ ($Re \simeq 3{\cdot}7 \times 10^3$) and calculations were stopped there without marching further downstream into the region of flow reversal.

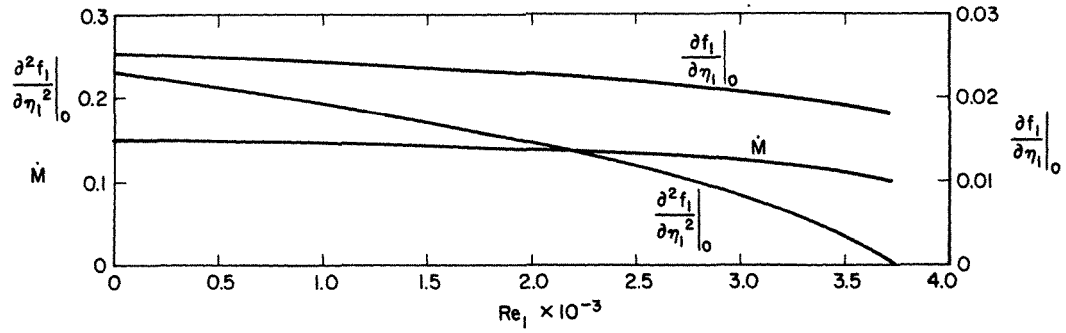

Figure 9. Interfacial parameters in a decelerating laminar flow ($u_\infty = 1 - \xi$, $T_\infty = 100\,^\circ\text{C}$, $T_{-\infty} = 80\,^\circ\text{C}$, $m_{v_\infty} = \gamma_1 = 0$). All symbols are the same as in Figure 8

Howarth[15] provided the first analytical solution to a linearly retarded laminar flow near separation and subsequent investigations have indicated that separation in this flow occurs at $\xi \simeq 0{\cdot}12$ on a flat plate.[16] In our simulation a finite, non-zero interfacial velocity, as well as surface evaporation, effectively reduce the shear stress and result in a separation point upstream of the value one obtains on a flat plate in the absence of surface mass transfer.

4. CONCLUSION

We have described a powerful and efficient numerical scheme for solving a broad class of boundary-layer problems involving laminar gas–liquid flow. We have presented the results of several computations and have examined effects of mild pressure gradient, a liquid current, and free-stream vapour concentration on parameters at the gas–liquid interface. In Appendix III we compare finite-difference computations of self-similar flows to solutions obtained by an algorithm employing Runge–Kutta integration. Agreement is excellent in all cases.

The finite-difference scheme which we have developed can be a useful computational tool for design engineers who wish to solve a variety of gas–liquid boundary-layer problems. Some applications were suggested in the Introduction.

ACKNOWLEDGEMENT

Support for this work was provided by U.S. National Science Foundation Grant ENG 79-01176 from the Heat Transfer Program of the Engineering Chemistry and Energetics Section and by Office of Naval Research Contract N00014-84-K-0242 of the Fluid Mechanics Division.

APPENDIX I: NOMENCLATURE

A, B, C	coefficient matrices
C_l	specific heat of liquid
C_p	constant pressure specific heat
D_1	$(d_1 - 1)(Sc^{-1} - Pr_l^{-1})(m_{v_0} - m_{v_\infty})$
d_1	C_{pv}/C_{pg}
D_2	$H/[1 + (d_1 - 1)m_v]^{-1}$
d_2	C_{pg}/C_l
d_3	L_v/i_∞
f	dimensionless stream function

Fr	Froude number, u_∞^2/gx
G	$\partial g/\partial \eta$
g	dimensionless enthalpy
H	$\partial h/\partial \eta$
h	dimensionless spacies concentration $(m_v - m_{v_\infty})/(m_{v_0} - m_{v_\infty})$
i	specific enthalpy
k	thermal conductivity
l_n	horizontal grid interval
L_v	latent heat of vaporization
$\dot{M}$	surface mass transfer rate
m_1	pressure-gradient parameter (gas)
m_2	pressure-gradient parameter (liquid)
m_v	mass fraction of vapour in the binary gas mixture
$\dot{m}''$	vapour flux
$\mathbf{P}$	block tridiagonal matrix
p	pressure; vertical grid spacing (Sections 2.2.1, 3)
Pr	Prandtl number
q	net function
R	residual function
$\mathbf{r}$	residual vector
R_v	molecular gas constant of liquid vapour
Re	Reynolds number based on steamwise distance
S	ratio of adjacent grid intervals in the vertical direction
s	surface displacement
Sc	Schmidt number
T	temperature
T_b	liquid boiling temperature at the ambient pressure of the gas-liquid system
T_r	reference temperature (0 °C)
u	horizontal velocity (Section 2.1, Appendix II); $\partial f/\partial \eta$ (Sections 2.2.1–2.2.2)
$u_\infty(x)$	free-stream velocity distribution
$u_{-\infty}(x)$	bulk liquid velocity distribution
v	vertical velocity (Section 2.1, Appendix II); $\partial^2 f/\partial \eta^2$ (Section 2.2.1, Appendix III)
x, y	horizontal and vertical co-ordinates, respectively

Greek symbols

α_n	$\xi^{n-1/2}/l_n$
$\boldsymbol{\delta}$	vector of unknowns
$\delta f, \delta u, \delta v$	iterates of differenced field variables (momentum problem)
γ	mass diffusion coefficient
γ_1	$u_{-\infty}/u_\infty$
γ_2	$i_{-\infty}/i_\infty$
Γ	thermal diffussion coefficient
ε	convergence parameter
θ	non-dimensional temperature
λ	tolerance parameter
Λ	density-viscosity ratio, $\sqrt{\left(\frac{\rho_2 \mu_2}{\rho_1 \mu_1}\right)}$
ξ, η	Falkner–Skan co-ordinates

μ	dynamic viscosity
ν	kinematic viscosity
ρ	density
ψ	stream function

Subscripts

1, 2	gas, liquid
$\infty, -\infty$	free stream and bulk liquid, respectively
e	enthalpy
g	(dry) gas
j, k	indices designating vertical grid point locations ($j = 0, 1, \ldots, J$; $k = 0, -1, \ldots, -K$)
0	interface
v	vapour

Superscripts

$'$	ordinary derivative
n	index designating horizontal grid point locations

APPENDIX II: THE MEAN-TRANSPORT EQUATIONS AND BOUNDARY CONDITIONS FOR COUPLED BOUNDARY-LAYER PROBLEMS

If the subscripts 1 and 2 refer, respectively, to the regimes above and below the interface, the differential equations governing the mean flow at steady state are given by

$$\frac{\partial u_1}{\partial x} + \frac{\partial v_1}{\partial y_1} = 0, \tag{15a}$$

$$\rho_1 u_1 \frac{\partial u_1}{\partial x} + \rho_1 v_1 \frac{\partial u_1}{\partial y_1} = -\frac{\partial p_1}{\partial x} + \frac{\partial}{\partial y_1}\left(\mu_1 \frac{\partial u_1}{\partial y_1}\right), \tag{15b}$$

$$0 = \frac{\partial p_1}{\partial y_1}, \tag{15c}$$

$$\rho_1 u_1 \frac{\partial i_1}{\partial x} + \rho_1 v_1 \frac{\partial i_1}{\partial y_1} = \frac{\partial}{\partial y_1}\left[\frac{(d_1 - 1) i_1}{1 + (d_1 - 1) m_v}(\gamma - \Gamma_1)\frac{\partial m_v}{\partial y_1} + \Gamma_1 \frac{\partial i_1}{\partial y_1}\right], \tag{15d}$$

$$\rho_1 u_1 \frac{\partial m_v}{\partial x} + \rho_1 v_1 \frac{\partial m_v}{\partial y_1} = \frac{\partial}{\partial y_1}\left(\gamma \frac{\partial m_v}{\partial y_1}\right), \tag{15e}$$

$$\frac{\partial u_2}{\partial x} + \frac{\partial v_2}{\partial y_2} = 0, \tag{15f}$$

$$\rho_2 u_2 \frac{\partial u_2}{\partial x} + \rho_2 v_2 \frac{\partial u_2}{\partial y_2} = -\frac{\partial p_2}{\partial x} + \frac{\partial}{\partial y_2}\left(\mu_2 \frac{\partial u_2}{\partial y_2}\right), \tag{15g}$$

$$0 = \frac{\partial p_2}{\partial y_2} - \rho_2 g, \tag{15h}$$

$$\rho_2 u_2 \frac{\partial i_2}{\partial x} + \rho_2 v_2 \frac{\partial i_2}{\partial y_2} = \frac{\partial}{\partial y_2}\left(\Gamma_2 \frac{\partial i_2}{\partial y_2}\right). \tag{15i}$$

The relevant boundary conditions at the gas–liquid interface (denoted by the subscript 0) are

$$-p_{1_0}+2\mu_1\left.\frac{\partial v_1}{\partial y_1}\right|_0=-p_{2_0}+2\mu_2\left.\frac{\partial v_2}{\partial y_2}\right|_0, \tag{16a}$$

$$u_{1_0}=u_{2_0}\equiv u_0, \tag{16b}$$

$$\mu_1\left.\frac{\partial u_1}{\partial y_1}\right|_0=\mu_2\left.\frac{\partial u_2}{\partial y_2}\right|_0, \tag{16c}$$

$$T_{1_0}=T_{2_0}\equiv T_0, \tag{16d}$$

$$\rho_1 v_{1_0}=\rho_2 v_{2_0}\equiv \dot{m}_0'', \tag{16e}$$

$$\dot{m}_0''=\left.\frac{\mu_1}{Sc(m_{v_0}-1)}\frac{\partial m_v}{\partial y_1}\right|_0, \tag{16f}$$

$$\dot{m}_0'' L_v-\left[\frac{(d_1-1)i_1}{1+(d_1-1)m_v}(\gamma-\Gamma_1)\frac{\partial m_v}{\partial y_1}+\Gamma_1\frac{\partial i_1}{\partial y_1}\right]\Bigg|_0+\Gamma_2\left.\frac{\partial i_2}{\partial y_2}\right|_0=0, \tag{16g}$$

$$m_{v_0}=\exp\left[\frac{L_v}{R_v}\left(\frac{1}{T_b}-\frac{1}{T_0}\right)\right]. \tag{16h}$$

Far-field boundary conditions are given by

$$u_1\to u_\infty,\quad i_1\to i_\infty,\quad m_v+m_{v_\infty}\quad \text{as } y_1\to\infty \tag{17a}$$

and

$$u_2\to u_{-\infty},\quad i_2\to i_{-\infty}\quad \text{as } y_2\to-\infty. \tag{17b}$$

Equations (16a)–(16d) are continuity relations at the interface for the normal stress, horizontal velocity, shear stress, and temperature, respectively. Equations (16e) and (16f) are mass-conservation relations, (16g) is an expression for the conservation of energy and (16h) is the Clausius–Clapeyron equation which relates the interfacial temperature and vapour concentration under conditions of thermodynamic equilibrium. Equations (16f) and (16g) were derived by applying the conservation principle to a control volume centred at the interface, by assuming that liquid vapour is the only transferred substance between the liquid and the binary gas, and by neglecting radiative heat transfer.

The specific enthalpies i_1 and i_2 are defined by

$$i_1=m_g i_g+m_v i_v,$$
$$i_2=C_l T_2-L_v,$$

where $i_g=C_{p_g}(T_1-T_r)$ and $i_v=C_{p_v}(T_1-T_r)$ are the corresponding component enthalpies, m_g and m_v are the mass fractions of dry gas and liquid vapour, respectively, and T_r is a reference temperature ($T_r=0\,^\circ\mathrm{C}$ in this analysis). The mass transport terms in (15d) and (16g) result from the heat flux, which can be written in the form

$$-k\frac{\partial T_1}{\partial y_1}=-\Gamma\left[\frac{\partial i_1}{\partial y_1}-\left(i_g\frac{\partial m_g}{\partial y_1}+i_v\frac{\partial m_v}{\partial y_1}\right)\right]$$

for a binary mixture, where k is the conductivity and Γ the thermal diffusion coefficient.

The pressure gradients in equations (15b) and (15g) are

$$-\frac{\partial p_1}{\partial x}=-\frac{\partial p_\infty}{\mathrm{d}x}=\rho_1 u_\infty\frac{\mathrm{d}u_\infty}{\mathrm{d}x} \tag{18a}$$

and

$$-\frac{\partial p_2}{\partial x} = -\frac{\mathrm{d}p_{-\infty}}{\mathrm{d}x} = \rho_2 u_{-\infty}\frac{\mathrm{d}u_{-\infty}}{\mathrm{d}x}. \tag{18b}$$

Because these gradients are determined from the far-field inviscid flow in each fluid regime, we need not compute the pressure field explicitly and we can disregard the normal stress boundary condition (16a) in solving the system (15) and (16).

Although pressure arises in no other context different pressure gradients above and below the interface preclude the interfacial boundary from remaining horizontal. Equations (15c) and (15h) imply that

$$\frac{\mathrm{d}p_{-\infty}}{\mathrm{d}x} = \frac{\mathrm{d}p_{2_0}}{\mathrm{d}x} + \rho_2 g\frac{\mathrm{d}s}{\mathrm{d}x}, \tag{19a}$$

and

$$\frac{\mathrm{d}p_{\infty}}{\mathrm{d}x} = \frac{\mathrm{d}p_{1_0}}{\mathrm{d}x}, \tag{19b}$$

where $s(x)$ is the vertical surface displacement from the horizontal axis. By subtracting (19b) from (19a) and using equations (16a) and (18), we obtain an expression for the surface tilt given by

$$\frac{\mathrm{d}s}{\mathrm{d}x} = Fr_1\frac{\rho_1}{\rho_2}m_1 - \gamma_1^2 m_2 + \frac{2x^2}{u_\infty}\left(\frac{\rho_1}{\rho_2}Re_1^{-1} - Re_2^{-1}\right)\left.\frac{\partial^2 u_1}{\partial x^2}\right|_0, \tag{20}$$

in which

$$Fr_1 = \frac{u_\infty^2}{gx}, \quad Re_1 = \frac{\rho_1 u_\infty x}{\mu_1}, \quad Re_2 = \frac{\rho_2 u_\infty x}{\mu_2}.$$

Only for the restricted class of self-similar laminar problems without pressure gradient is $\mathrm{d}s/\mathrm{d}x = 0$; such problems were investigated by Lock[2] and Kotake.[3]

In laminar gas–liquid flows $\mathrm{d}s/\mathrm{d}x$ is typical $O(10^{-4})$ or smaller and its effect can be neglected. Incorporating surface tilt in our analysis would require that we modify the field equations in order to account for boundary-layer curvature (since, in general, $\mathrm{d}^2 s/\mathrm{d}x^2 \neq 0$) and gravitational acceleration. We would then use equation (20) in a particular problem to determine the displacement $s(x)$ and to align the x-axis of the co-ordinate system with the predominant flow direction; u and v would correspond to velocity components parallel and perpendicular to the interfacial boundary, respectively.

APPENDIX III: THE SOLUTION OF SELF-SIMILAR LAMINAR FLOWS AT A SMOOTH, PHASE-CHANGING INTERFACE BY RUNGE–KUTTA INTEGRATION

Self-similar gas–liquid problems can be solved by Runge–Kutta integration and solutions so obtained then compared to those computed by the finite-difference algorithm described in Section 2. This comparison allows us to assess the accuracy of the latter method.

Klotz and Street[11] provide details of the Runge–Kutta algorithm which we used to compute solutions. In it the momentum equations above and below the interface are solved using the variational scheme described by Cebeci and Bradshaw[9] and Keller.[18] The procedure involves iterating by Newton's method on estimates of the surface velocity and shear stress in order to satisfy all far-field boundary conditions. Since the momentum problem is coupled to the heat and mass transfer problems, f_{1_0} is calculated by solving the latter in each iteration.

Table III. Computed interfacial parameters for several self-similar flows (air–water systems)

					Fourth-order Runge–Kutta						Finite difference					
T_∞ (°C)	$T_{-\infty}$ (°C)	m_1	γ_1	m_{v_∞}	η_∞	$\eta_{-\infty}$	f'_{1_0}	f''_{1_0}	$\dot{M}$	T_0 (°C)	η_∞	$\eta_{-\infty}$	f'_{1_0}	f''_{1_0}	$\dot{M}$	T_0 (°C)
100	80	0	0	0	9	−64	0·02518	0·2310	0·1506	68·26	10	−128	0·02518	0·2309	0·1506	68·26
		0	0·2	0	8	−24	0·2059	0·1957	0·2311	74·43	9	−48	0·2059	0·1957	0·2311	74·43
		−0·05	0·1	0·2	8	−48	0·1248	0·1072	0·1417	75.77	10	−64	0·1248	0·1072	0·1416	75·78
10	20	0	0	0	8	−64	0·02312	0·3257	0·008740	19·03	10	−128	0·02312	0·3255	0·008740	19·03
		0	0	0·01	8	−64	0·02327	0·3288	0·004279	19·45	10	−128	0·02327	0·3286	0·004278	19·44

To compute the solutions discussed in this appendix we neglected the underlined terms in equations (1b) and (2g) which represent transport of enthalpy as the result of a species-concentration gradient above the gas–liquid interface. The equations governing scalar transport in self-similar flows can then be readily solved by quadrature[3] and improved estimates of T_0, m_{v_0} and f_{1_0} obtained directly from the interfacial boundary conditions.

Gas–liquid properties, the locations of η_∞ and $\eta_{-\infty}$ and initial estimates of f'_{1_0}, f''_{1_0}, g'_{1_0}, h'_0 and T_0 must be provided to start Runge–Kutta calculations. Solution convergence in our algorithm is not quadratic, which is characteristic of Newton's method, because g'_{1_0}, g_{1_0}, h'_0, T_0 and f_{1_0} are determined by successive approximation.

Table III contains computed values of the interfacial velocity f'_{1_0}, shear stress f''_{1_0}, surface temperature T_0 and mass-transfer rate $\dot{M}$ in several problems involving the air–water system. In all simulations gas–liquid properties were evaluated at the corresponding far-field temperature.

We used a fourth-order Runge–Kutta integrator to calculate the solutions presented here. This scheme automatically adjusted step size to control errors and is more accurate than the finite-difference method. It generally suffers, however, from the necessity of specifying initial values of all surface parameters and poor estimates of these may adversely affect the rate of solution convergence.

Convergence may also be influenced by the choice of η_∞ or $\eta_{-\infty}$ in a particular problem; in fact, if either of these parameters is too large, solutions computed by Runge–Kutta integration may diverge. Convergent solutions in which $|f''_{1_\infty}|$ and $|f''_{2_{-\infty}}|$ are small and have no effect on the magnitudes of computed interfacial parameters were obtained using the values of η_∞ and $\eta_{-\infty}$ recorded in Table III. In all cases $|f''_{1_\infty}| \leqslant 10^{-3}$ and $|f''_{2_{-\infty}}| \leqslant 10^{-5}$.

The computational grid which we use with the finite-difference method was described in Section 3 and in computing solutions with this scheme we assumed that $S_1 = 1{\cdot}02$, $\eta_{1_1} = 0{\cdot}1$, $S_2 = 1{\cdot}05$ and $\eta_{2_{-1}} = -0{\cdot}05$. This algorithm is not nearly as sensitive as is the Runge–Kutta method to the choice of η_∞ and $\eta_{-\infty}$. Solutions calculated using the values of η_∞ and $\eta_{-\infty}$ contained in Table III resulted in $|v_{1_J}| \leqslant 10^{-5}$ and $|v_{2_{-K}}| \leqslant 10^{-7}$ in all cases. Differences in interfacial parameters computed by each scheme and listed in Table III are limited to one or two digits in the last significant figure.

REFERENCES

1. L. C. Chow and J. N. Chung, 'Evaporation of water into a laminar stream of air and superheated steam', *Int. J. Heat Mass Transfer*, **26**, 373–380 (1983).
2. R. C. Lock, 'The velocity distribution in the laminar boundary layer between parallel streams', *Quart. J. Mech. and App. Math.*, **4**, (1), 42–63 (1951).
3. S. Kotake, 'Heat transfer and skin friction of a phase-changing interface of gas-liquid laminar flows', *Int. J. Heat Mass Transfer*, **16**, 2165–2176 (1973).
4. J. Schröppel and F. Thiele, 'Numerical method for the calculation of binary gas mixture condensation in boundary layer flow', *Proc. First Int. Conf. on Numerical Methods in Laminar and Turbulent Flow*, Wiley, New York, 1978, pp. 411–420.
5. R. L. Street, 'Turbulent heat and mass transfers across a rough air-water interface: a simple theory', *Int. J. Heat Mass Transfer*, **22**, 885–899 (1979).
6. W. T. Liu, K. B. Katsaros and J. A. Businger, 'Bulk parameterization of air-sea exchanges of heat and water vapor including the molecular constraints at the interface', *J. Atm. Sci.*, **36**, 1722–1735 (1979).
7. H. B. Keller and T. Cebeci, 'Accurate numerical methods for boundary layer flows. I. Two-dimensional laminar flows', in *Lecture Notes in Physics, 8, Proc. Second Int. Conf. on Numerical Methods in Fluid Dynamics*, Springer-Verlag, Berlin and New York, 1971, pp. 92–100.
8. T. Cebeci and A. M. O. Smith, *Analysis of Turbulent Boundary Layers*, Academic Press, New York, 1974.
9. T. Cebeci and P. Bradshaw, *Momentum Transfer in Boundary Layers*, McGraw-Hill Book Co., New York, 1977.
10. H. B. Keller, 'Numerical methods in boundary-layer theory', *Ann. Rev. Fluid Mech.*, **10**, 417–433 (1978).
11. S. P. Klotz and R. L. Street, 'Methods for simulating laminar boundary layers at a phase-changing, gas-liquid interface', *TR-286*, Dept. of Civil Engineering, Stanford University, Stanford, CA 94305, 1984.
12. E. Isaacson and H. B. Keller, *Analysis of Numerical Methods*, Wiley, New York, 1966.
13. H. B. Keller, 'Accurate difference methods for nonlinear two-point boundary-value problems', *SIAM J. Num. Anal.*, **11**, 305–320 (1974).

14. N. B. Vargaftik, *Tables on the Thermophysical Properties of Liquids and Gases*, 2nd edn., Hemisphere Publishing Corporation, Washington, D.C., 1975.
15. L. Howarth, 'On the solution of the laminar boundary layer equations', *Proc. Roy. Soc. London*, **A164,** 547–579 (1938).
16. F. M. White, *Viscous Fluid Flow*, McGraw-Hill Book Co., New York, 1974.
17. W. M. Kays and M. E. Crawford, *Convective Heat and Mass Transfer*, 2nd edn., McGraw-Hill Book Co., New York, 1980.
18. H. B. Keller, *Numerical Methods for Two-Point Boundary-Value Problems.* Blaisdell Publishing Co., Waltham, Massachusetts, 1968.